Multi-timescale Coordinated Distributed Energy Resource Control Combining Local and Online Feedback Optimization

Sen Zhan*, Johan Morren*†, Wouter van den Akker*‡, Anne van der Molen*§,
Nikolaos G. Paterakis*, J. G. Slootweg*†
* Eindhoven University of Technology, Eindhoven, The Netherlands; †Enexis, 's-Hertogenbosch, The Netherlands
‡Alliander, Arnhem, The Netherlands; §Stedin, Rotterdam, The Netherlands
Emails: {s.zhan, j.morren, w.f.v.d.akker, a.e.v.d.molen, n.paterakis, j.g.slootweg}@tue.nl

***Abstract*—Recently, online feedback optimization (OFO) emerges as a promising approach for real-time distribution grid management. OFO offers several advantages, including not requiring precise grid models or real-time load metering and demonstrating robustness against inaccurate problem data. However, one important limitation is that OFO does not consider the intertemporal relationships and short-term planning capabilities of assets, thus not harnessing the full potential of a variety of distributed energy resources (DER) such as batteries and electric vehicles. To address this limitation, this paper proposes a multi-timescale coordinated control framework. In the slower timescale, local optimization problems are solved to provide real-time OFO controllers with reference setpoints. The overall approach thereby maintains minimal model, computation, and communication requirements while enforcing grid limits. Case studies based on a 96-bus unbalanced low-voltage grid with a high DER penetration and second-scale data demonstrate its effectiveness and solution quality benchmarked with a centralized optimal power flow approach.**

***Index Terms*—Distribution grid management, local optimization, multiple timescales, online feedback optimization, primal-dual gradient projection**

I. Introduction

The proliferation of distributed energy resources (DER) such as photovoltaics (PV), electric vehicles (EV), and battery storage in distribution grids is expected to cause frequent voltage and congestion issues. Before turning to costly and time-consuming grid expansion, it is imperative to fully exploit flexibility from these DER to meet distribution grid limits while minimizing the impact on end-users. To achieve this, an efficient and effective DER coordination mechanism is essential. While optimal power flow (OPF) offers a flexible modeling framework, its applicability in distribution grids is considered limited in the real-time operational context. Constructing and solving OPF problems requires precise distribution grid models, load metering of individual end-users, and sufficient computational resources, which can all be difficult to acquire for distribution system operators (DSO).

To circumvent these difficulties, recent works in [1]–[12] proposed to integrate real-time voltage and power flow measurements into online optimization schemes such as gradient projection, leading to online feedback optimization (OFO); see also our earlier survey paper [13]. OFO presents several merits. First, it does not require precise grid models which are largely unavailable to DSO [14]. What is required are input-output sensitivities such as power-to-voltage sensitivities. Recent works have developed model-free OFO by introducing data-driven methods to estimate the input-output sensitivities online [15]–[17] or resorting to zeroth-order optimization [18]–[20]. Furthermore, it does not need load metering which is often unavailable either due to privacy concerns or regulatory restrictions. Finally, OFO demonstrates robustness to inaccurate problem data such as generation and load uncertainties, measurement noises, and intermittent and delayed communication [21], [22]. These characteristics render it particularly suitable for real-time distribution grid management; see [23]–[25] for some experimental works.

Despite its various benefits, one important limitation of OFO is that it is based on real-time measurements and immediate response. Therefore, it does not consider the intertemporal relationships of assets. So far, this has limited its application primarily to reactive power or PV control. The study in [5] also considered EV and battery storage, where EV follows their maximum charging rates and batteries are minimally used (i.e. following zero setpoints). This fails to utilize the full potential of batteries. For example, batteries can be strategically planned to charge over the day to supply EV demand in peak hours, or discharge over the night to accommodate surplus PV generation. Augmenting OFO controllers with such short-term planning capabilities will create new possibilities for controlling a variety of DER.

The research question this paper aims to address is how we can effectively leverage OFO to control DER with intertemporal relationships to fully utilize their capabilities. To evaluate the effectiveness, the impact on end-users such as generation curtailment and load shedding and the contribution

This work is funded by TKI Energie from the 'Toeslag voor Topconsortia voor Kennis en Innovatie (TKI)' from the Ministry of Economic Affairs and Climate, under reference 1821401.

to grid constraint satisfaction are considered. To this end, this paper proposes a multi-timescale coordinated DER control framework. In the slower timescale, such as day-ahead or near real time on a rolling basis, DER scheduling within each household is locally optimized with the objective to smoothen individual net load profiles, see e.g. [26], [27]. This is expected to relieve network congestion. In real time, OFO controllers are deployed. To coordinate the different timescales, the optimized scheduling decisions in the slower timescale are used as reference setpoints for real-time OFO controllers. The strategic choice of local optimization maintains minimum grid model, computation, and communication requirements. Furthermore, OFO complements local optimization by ensuring that voltage and loading limits are kept in real-time grid operation.

Multi-timescale coordinated control approaches have already been explored in the literature. For instance, [28], [29] studied voltage/var control across various timescales incorporating local droop control in real time. Nevertheless, due to the lack of coordination, droop controllers cannot pursue grid-level objectives and do not guarantee the desired voltage regulation [7]. In [11], forecast-based optimization of on-load tap changers and OFO-based reactive power control were coordinated for voltage regulation. While their work also explored OFO in a multi-timescale context, different assets are dispatched across different timescales. Unlike our focus on extending the capability of OFO to manage DER with intertemporal relationships, OFO in their case only controls reactive power from PV, which is temporally decoupled. To summarize, our main contributions are the following:

- We propose a multi-timescale coordinated approach for OFO to control DER with intertemporal dependencies such as batteries and EV to harness their full potential. Optimization problems at the slower timescale are solved to provide OFO controllers with reference setpoints.
- With local optimization employed at the slower timescale, the overall approach maintains minimal grid model, computation, and communication requirements while enforcing distribution grid limits.

The remainder of this paper is organized as follows: Section II describes the coordinated control architecture across multiple timescales and local optimization. Section III presents the online feedback optimization approach. Case studies are reported in Section IV, while Section V concludes this study.

II. Multi-timescale Coordinated Control

A. Multi-timescale coordination framework

To address the research question, we propose a multi-timescale coordinated control framework. Fig. 1 illustrates its communication process. In the slower timescale, local optimization problems, which provide real-time controllers with reference setpoints, are solved without any communication requirement. In the faster timescale, OFO controllers, which are enabled by inverter-interfaced fast-reacting DER such as PV, EV, and batteries, enforce distribution grid limits while attempting to track the given setpoints using the gather-and-broadcast communication architecture [18]. In this work, we employ an OFO approach using the primal-dual gradient projection (PDGP) algorithm [4], [5], which features distributed implementation and light communication requirements. Note that the main contribution of this work, i.e. combining local and online feedback optimization, provides a general framework. While local optimization can include various technical and economic optimization schemes, OFO can also be implemented with different algorithms and to address different network issues [13].

B. Local optimization

In this section, we present a standard model of batteries and our local optimization scheme. Let $\mathcal{T} = \{1, 2, \cdots, T\}$ represent time steps in the local optimization horizon and Δt each time step length. Consider a battery storage unit, at each time step $t \in \mathcal{T}$, let $p^{ch,t}$ and $p^{dis,t}$ denote its charging and discharging power, respectively. Introduce δ^t as a binary variable regulating the charging and discharging status, and let E^t represent its energy content and E^{st} its energy capacity. Define S^{st} as its power rating, and η^{ch} and η^{dis} as the charging and discharging efficiencies, respectively. Finally, consider SoC^0 as the initial state of charge (SoC), and $\underline{\text{SoC}}$ and $\overline{\text{SoC}}$ as its lower and upper limits.

We present an operational model for batteries in (1). Constraints (1a) and (1b) ensure that batteries do not charge and discharge simultaneously. Equation (1c) models the energy content, considering charging and discharging losses. Finally, SoC limits are imposed in (1d) and (1e).

$$\delta^t \in \{0, 1\}, \forall t \in \mathcal{T}, \tag{1a}$$

$$0 \leq p^{ch,t} \leq \delta^t S^{st}, 0 \leq p^{dis,t} \leq (1 - \delta^t) S^{st}, \forall t \in \mathcal{T}, \tag{1b}$$

$$E^t = E^{t-1} + (\eta^{ch} p^{ch,t} - \frac{p^{dis,t}}{\eta^{dis}}) \Delta t, \forall t \in \mathcal{T}, \tag{1c}$$

$$E^0 = E^T = \text{SoC}^0 E^{st}, \tag{1d}$$

$$\underline{\text{SoC}} E^{st} \leq E^t \leq \overline{\text{SoC}} E^{st}, \forall t \in \mathcal{T}. \tag{1e}$$

Given local generation and demand profiles $p^{g,t}$ and $p^{d,t}$ respectively, the local optimization problem can be formulated as (2). The objective function can be chosen as the distance between the net load $\mathbf{p}$ and a desired zero load $\mathbf{0}$ using any vector norm $f(\mathbf{p}) = \|\mathbf{p} - \mathbf{0}\|$. A convenient modeling choice is the Euclidean norm.

$$\min_{p^{ch,t}, p^{dis,t}} f(\underbrace{[p^{ch,t} - p^{dis,t} + p^{d,t} - p^{g,t}, \forall t \in \mathcal{T}]^\intercal}_{\text{Net load } \mathbf{p}}) \tag{2}$$

$$\text{s. t. Battery model } (1).$$

Remark 1: While the multi-period OPF approach can also be used which conducts network-level optimization, it encounters several challenges when applied to distribution grids. First, it relies on precise knowledge of distribution grid topologies. Second, it necessitates communication of load data at individual households, which also introduces privacy concerns. Finally, large grids pose scalability issues.

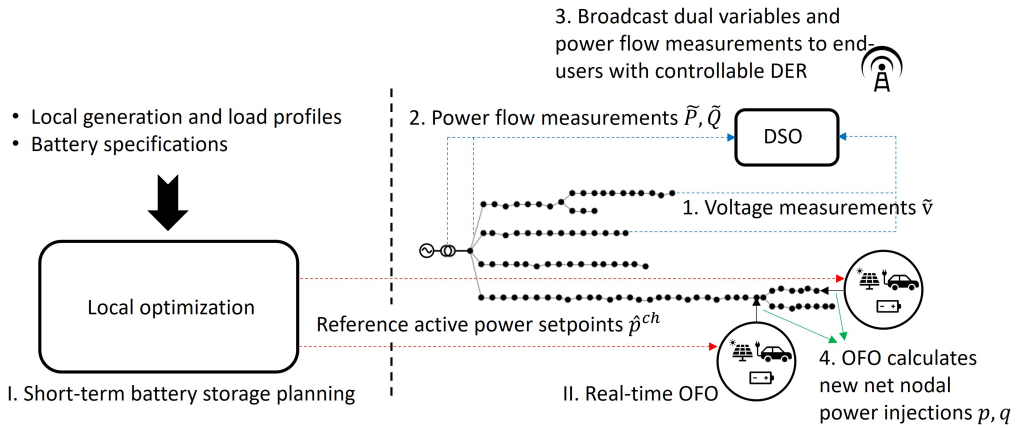

Fig. 1. Multi-timescale coordinated control framework.

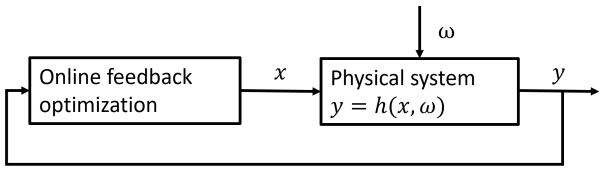

Fig. 2. Block diagram of a closed-loop feedback system, where x represents system input, y represents system output, ω represents system disturbance, and h maps system input and disturbance to system output. Figure adapted from [25]. See [25] for comparison to a model-based feedforward system.

Remark 2: In real time, OFO controllers dispatch PV, EV, and batteries. In the local planning stage, we focus on batteries in this work. For EV, our primary objective is to ensure the fulfillment of their energy demand. Therefore, their maximum charging rates are used as reference setpoints for OFO in real time. In the local optimization stage, they are regarded as loads operating at an uncontrolled charging mode (charging at their maximum rates when plugged in). In a dynamic pricing context, EV might be charged with a cost minimization objective. Accordingly, they can be integrated into a profit-driven local planning to provide OFO controllers with economically favorable reference setpoints.

III. Online Feedback Optimization Framework

In this section, we present the OFO framework based on the PDGP algorithm, which features distributed implementation. Notations, a real-time optimization problem, and the PDGP algorithm which is designed to solve this problem in a feedback-based manner are presented below.

A. Notation

Consider a distribution grid with $N+1$ buses collected in the set $\mathcal{N} = \{0, 1, \cdots, N\}$, and cables represented by the set $\mathcal{E} = \{(i,j)\} \subset \mathcal{N} \times \mathcal{N}$. Denote a cable in $\mathcal{E}$ by an ordered pair (i,j) if it points from bus i to bus j. Define $\mathcal{N}^+ = \mathcal{N} \backslash \{0\}$. Bus 0 is the substation bus. Use $\Phi = \{a, b, c\}$ to denote the three phases, and use ϕ or ψ to refer to any one of them. Since the algorithm is based on real-time information, we drop the time index t in the following notations. For each bus $j \in \mathcal{N}$, let $v_{j,\phi}$ be the magnitude of the complex voltage phasor for phase ϕ, and let $\underline{v}$ and $\overline{v}$ be the lower and upper limits, respectively. Bus 0 has a fixed voltage magnitude of v_0. For each cable $(i,j) \in \mathcal{E}$, denote by $P_{ij,\phi}$ and $Q_{ij,\phi}$ the active and reactive power flows from bus i to j for phase ϕ, and by $S^{cable}_{ij,\phi}$ its rated capacity. Denote by $r_{ij,\phi\psi}$ and $x_{ij,\phi\psi}$ the resistance and reactance between phase ϕ of bus i and phase ψ of bus j, and S^{trafo}_{ϕ} the transformer capacity for phase ϕ.

For each bus $j \in \mathcal{N}$ and phase $\phi \in \Phi$, let $p_{j,\phi}$ and $q_{j,\phi}$ be the net active and reactive power injections for controllable assets, respectively. Let $S^{pv}_{j,\phi}$ and $\hat{p}^{pv}_{j,\phi}$ be the PV inverter capacity and maximum PV generation. Let $S^{ev}_{j,\phi}$ be the maximum charging rate and $\delta^{ev}_{j,\phi}$ represents if an EV is plugged in. Let $\Delta E^{ev}_{j,\phi}$ be the remaining energy demand and δt hereafter be the time length of an OFO iteration. Let $\hat{p}^{ch}_{j,\phi} = (p^{ch,t})^* - (p^{dis,t})^*$ be the planned battery charging rate computed in the local optimization stage, where $(p^{ch,t})^*$ and $(p^{dis,t})^*$ are the solution to (2) for the battery located at phase ϕ of bus j for the corresponding time step t.

B. Preliminaries

Fundamentally, OFO provides a real-time feedback-based solution approach of the optimization problem (3); see Fig. 2 for a sketch of a closed-loop feedback system. The decision variables $p_{j,\phi}, q_{j,\phi}$ are the nodal net active and reactive power injections respectively, realized by DER such as PV, EV, and batteries owned by individual end-users connected to the specific node. The objective function (3a) minimizes active power deviations from the reference setpoints $\hat{p}_{j,\phi}$ and reactive power use, where ξ is a sufficiently small weighting factor to prioritize reactive power use. Specifically, $\hat{p}_{j,\phi} = \hat{p}^{pv}_{j,\phi} - \delta^{ev} S^{ev}_{j,\phi} - \hat{p}^{ch}_{j,\phi}$ represents the reference setpoint for nodal net active power injection.

$$\min g = \min_{p_{j,\phi}, q_{j,\phi}} \sum_{j \in \mathcal{N}} \sum_{\phi \in \Phi} \left[(p_{j,\phi} - \hat{p}_{j,\phi})^2 + \xi (q_{j,\phi})^2 \right], \quad \text{(3a)}$$

$$\text{s. t. } [p_{j,\phi}, q_{j,\phi}]^\intercal \in \mathcal{X}_{j,\phi}, \forall j \in \mathcal{N}, \forall \phi \in \Phi, \quad \text{(3b)}$$

$$\underline{v} \leq v_{j,\phi} \leq \overline{v} : \mu_{j,\phi}, \lambda_{j,\phi}, \forall j \in \mathcal{N}^+, \forall \phi \in \Phi, \quad \text{(3c)}$$

$$\frac{\sqrt{P_{ij,\phi}^2+Q_{ij,\phi}^2}}{S_{ij,\phi}^{cable}} \le 1 : \rho_{ij,\phi}, \forall (i,j) \in \mathcal{E}, \forall \phi \in \Phi, \tag{3d}$$

$$\frac{\sqrt{(P_{\phi}^{trafo})^2+(Q_{\phi}^{trafo})^2}}{S_{\phi}^{trafo}} \le 1 : \pi_{\phi}, \forall \phi \in \Phi. \tag{3e}$$

The feasibility of nodal net power injections is enforced in (3b), where $\mathcal{X}_{j,\phi}$ is defined in (4). Finally, (3c)-(3e) impose limits on bus voltages and loadings of cables and the transformer, respectively, where $\mu_{j,\phi}$, $\lambda_{j,\phi}$, $\rho_{ij,\phi}$, and π_{ϕ} represent the respective dual variables. Note that the voltages and loadings are dependent, through an implicit function, on the decision variables $p_{j,\phi}$ and $q_{j,\phi}$ and non-controllable loads.

$$\begin{aligned}\mathcal{X}_{j,\phi} = \Big\{ [p,q]^{\intercal} : \; & p = p^{pv} - p^{ev} - p^{ch}, q = q^{pv} - q^{ev} - q^{ch}, \\ & (p^{pv})^2 + (q^{pv})^2 \le (S_{j,\phi}^{pv})^2, 0 \le p^{pv} \le \hat{p}_{j,\phi}^{pv}, \\ & (p^{ev})^2 + (q^{ev})^2 \le (S_{j,\phi}^{ev})^2, 0 \le p^{ev} \le \delta^{ev} S_{j,\phi}^{ev}, \\ & p^{ev} \le \frac{\Delta E_{j,\phi}^{ev}}{\Delta t}, (p^{ch})^2 + (q^{ch})^2 \le (S_{j,\phi}^{st})^2 \\ & \eta^{dis} \frac{\underline{\text{SoC}} E_{j,\phi}^{st} - E_{j,\phi}^{t-1}}{\Delta t} \le p^{ch} \le \frac{\overline{\text{SoC}} E_{j,\phi}^{st} - E_{j,\phi}^{t-1}}{\eta^{ch} \Delta t} \Big\}. \end{aligned} \tag{4}$$

Let $\boldsymbol{\lambda} = [\lambda_{1,a}, \lambda_{1,b}, \lambda_{1,c}, \cdots, \lambda_{N,a}, \lambda_{N,b}, \lambda_{N,c}]^{\intercal}$ collect the dual variables $\lambda_{j,\phi}$ for each bus $j \in \mathcal{N}^+$ and phase $\phi \in \Phi$. Likewise, let $\boldsymbol{\mu}$, $\boldsymbol{\rho}$, and $\boldsymbol{\pi}$ collect the respective dual variables, and let $\mathbf{p}$ and $\mathbf{q}$ collect the nodal net active and reactive power injections. Define $\mathbf{v} = [v_{1,a}, v_{1,b}, v_{1,c}, \cdots, v_{N,a}, v_{N,b}, v_{N,c}]^{\intercal}$ which collects bus voltages excluding the substation bus. Define $\mathbf{1} = [1, 1, \cdots, 1]^{\intercal}$ as a vector of ones with a proper dimension. The primal-dual gradient projection algorithm iterates between gradient projection steps for primal and dual variables for the saddle-point problem (5).

$$\max_{\substack{\boldsymbol{\lambda} \ge \mathbf{0}, \boldsymbol{\mu} \ge \mathbf{0}, \\ \boldsymbol{\rho} \ge \mathbf{0}, \boldsymbol{\pi} \ge \mathbf{0}}} \Big\{ \min_{\substack{(p_{j,\phi}, q_{j,\phi}) \in \mathcal{X}_{j,\phi}, \\ \forall \phi \in \Phi, \forall j \in \mathcal{N}}} \mathcal{L}(\mathbf{p}, \mathbf{q}, \boldsymbol{\lambda}, \boldsymbol{\mu}, \boldsymbol{\rho}, \boldsymbol{\pi}) \Big\}, \tag{5}$$

where the Lagrangian function is defined in (6). While several papers such as [4], [5] leveraged primal and dual regularization terms to establish convergence results, we found in our simulations that the algorithm works well without regularization.

$$\begin{aligned}\mathcal{L}(\mathbf{p}, \mathbf{q}, \boldsymbol{\lambda}, \boldsymbol{\mu}, \boldsymbol{\rho}, \boldsymbol{\pi}) = & \; g + \boldsymbol{\lambda}^{\intercal}(\mathbf{v} - \overline{v}\mathbf{1}) - \boldsymbol{\mu}^{\intercal}(\mathbf{v} - \underline{v}\mathbf{1}) \\ & + \sum_{(i,j) \in \mathcal{E}, \phi \in \Phi} \rho_{ij,\phi} \left(\frac{\sqrt{P_{ij,\phi}^2 + Q_{ij,\phi}^2}}{S_{ij,\phi}^{cable}} - 1 \right) \\ & + \sum_{\phi \in \Phi} \pi_{\phi} \left(\frac{\sqrt{(P_{\phi}^{trafo})^2 + (Q_{\phi}^{trafo})^2}}{S_{\phi}^{trafo}} - 1 \right). \end{aligned} \tag{6}$$

C. Primal-dual gradient projection (PDGP) algorithm

In this section, we present an implementation of OFO based on the PDGP algorithm. While other algorithms such as gradient projection are available, PDGP features distributed calculations, which makes it attractive for distribution grids. The algorithm is built upon a gather-and-broadcast communication architecture.

Let $\alpha > 0$ with a proper superscript be the step size, e.g., α^{λ} for $\boldsymbol{\lambda}$ update. Let letters with a tilde symbol be the corresponding measurements, e.g., $\tilde{v}_{j,\phi}$ for the voltage measurement for bus j and phase ϕ. Let $[\cdot]^+$ be the projection operator onto the nonnegative orthant. At each time step (iteration) k, the algorithm includes four steps:

Step 1: For each bus $j \in \mathcal{N}^+$ and phase $\phi \in \Phi$ with a voltage measurement unit $(j,\phi) \in \tilde{\mathcal{M}}_v \subset \mathcal{N} \times \Phi$, collect the voltage measurement $\tilde{v}_{j,\phi}^k$, update $\lambda_{j,\phi}$ and $\mu_{j,\phi}$ locally, and send the updated $\lambda_{j,\phi}^{k+1}$ and $\mu_{j,\phi}^{k+1}$ to the DSO.

$$\lambda_{j,\phi}^{k+1} \leftarrow \left[\lambda_{j,\phi}^k + \alpha^{\lambda} (\tilde{v}_{j,\phi}^k - \overline{v}) \right]^+, \tag{7a}$$

$$\mu_{j,\phi}^{k+1} \leftarrow \left[\mu_{j,\phi}^k + \alpha^{\mu} (\underline{v} - \tilde{v}_{j,\phi}^k) \right]^+. \tag{7b}$$

Step 2: For each cable of interest $\tilde{\mathcal{E}} \subseteq \mathcal{E}$ and the transformer and phase $\phi \in \Phi$, the DSO collects active and reactive power flow measurements $\tilde{P}_{ij,\phi}^k$, $\tilde{Q}_{ij,\phi}^k$, $(\tilde{P}_{\phi}^{trafo})^k$, and $(\tilde{Q}_{\phi}^{trafo})^k$ and updates $\rho_{ij,\phi}$ and π_{ϕ}, where $\tilde{S}_{ij,\phi}^k = \sqrt{(\tilde{P}_{ij,\phi}^k)^2 + (\tilde{Q}_{ij,\phi}^k)^2}$, $(\tilde{S}_{\phi}^{trafo})^k = \sqrt{((\tilde{P}_{\phi}^{trafo})^k)^2 + ((\tilde{Q}_{\phi}^{trafo})^k)^2}$.

$$\rho_{ij,\phi}^{k+1} \leftarrow \left[\rho_{ij,\phi}^k + \alpha^{\rho} \left(\frac{\tilde{S}_{ij,\phi}^k}{S_{ij,\phi}^{cable}} - 1 \right) \right]^+, \tag{8a}$$

$$\pi_{\phi}^{k+1} \leftarrow \left[\pi_{\phi}^k + \alpha^{\pi} \left(\frac{(\tilde{S}_{\phi}^{trafo})^k}{S_{\phi}^{trafo}} - 1 \right) \right]^+. \tag{8b}$$

Step 3: The DSO broadcasts the above dual variables and power flow measurements of cables and the transformer.

Step 4: For each bus $j \in \mathcal{N}$ and phase $\phi \in \Phi$, update the active and reactive power setpoints $p_{j,\phi}$ and $q_{j,\phi}$ locally.

$$\begin{aligned} \dot{p}_{j,\phi}^{k+1} \leftarrow & \; p_{j,\phi}^k - \alpha \Bigg\{ (\frac{\partial g}{\partial p_{j,\phi}})^k \\ & + \sum_{(i,\psi) \in \tilde{\mathcal{M}}_v} \left[(\lambda_{i,\psi}^{k+1} - \mu_{i,\psi}^{k+1}) \frac{\partial v_{i,\psi}}{\partial p_{j,\phi}} \right] \\ & + \sum_{(m,n) \in \tilde{\mathcal{E}}, \psi \in \Phi} \left[\frac{\rho_{mn,\psi}^{k+1} \tilde{P}_{mn,\psi}^k}{\tilde{S}_{mn,\psi}^k S_{mn,\psi}^{cable}} \frac{\partial P_{mn,\psi}}{\partial p_{j,\phi}} \right] \\ & + \sum_{\psi \in \Phi} \left[\frac{\pi_{\psi}^{k+1} (\tilde{P}_{\psi}^{trafo})^k}{(\tilde{S}_{\psi}^{trafo})^k S_{\psi}^{trafo}} \frac{\partial P_{\psi}^{trafo}}{\partial p_{j,\phi}} \right] \Bigg\}, \end{aligned} \tag{9a}$$

$$\begin{aligned} \dot{q}_{j,\phi}^{k+1} \leftarrow & \; q_{j,\phi}^k - \alpha \Bigg\{ (\frac{\partial g}{\partial q_{j,\phi}})^k \\ & + \sum_{(i,\psi) \in \tilde{\mathcal{M}}_v} \left[(\lambda_{i,\psi}^{k+1} - \mu_{i,\psi}^{k+1}) \frac{\partial v_{i,\psi}}{\partial q_{j,\phi}} \right] \\ & + \sum_{(m,n) \in \tilde{\mathcal{E}}, \psi \in \Phi} \left[\frac{\rho_{mn,\psi}^{k+1} \tilde{Q}_{mn,\psi}^k}{\tilde{S}_{mn,\psi}^k S_{mn,\psi}^{cable}} \frac{\partial Q_{mn,\psi}}{\partial q_{j,\phi}} \right] \\ & + \sum_{\psi \in \Phi} \left[\frac{\pi_{\psi}^{k+1} (\tilde{Q}_{\psi}^{trafo})^k}{(\tilde{S}_{\psi}^{trafo})^k S_{\psi}^{trafo}} \frac{\partial Q_{\psi}^{trafo}}{\partial q_{j,\phi}} \right] \Bigg\}, \end{aligned} \tag{9b}$$

$$[p_{j,\phi}^{k+1}, q_{j,\phi}^{k+1}] \leftarrow \text{proj}_{\mathcal{X}_{j,\phi}^k} [\dot{p}_{j,\phi}^{k+1}, \dot{q}_{j,\phi}^{k+1}]. \tag{9c}$$

To finalize the gradient computations in (9a) and (9b), we must define the partial derivatives for voltages and power flows. To achieve this, we leverage the linearized power flow relations in (10), which are established assuming nearly balanced voltages and lossless cables [30], [31].

$$\mathbf{v} = v_0\mathbf{1} + \mathbf{R}(\mathbf{p^g} - \mathbf{p^c}) + \mathbf{X}(\mathbf{q^g} - \mathbf{q^c}), \tag{10a}$$

$$P_{ij,\phi} = \sum_{k\in\beta(j)} (p^c_{k,\phi} - p^g_{k,\phi}), \forall (i,j) \in \mathcal{E}, \forall \phi \in \Phi, \tag{10b}$$

$$Q_{ij,\phi} = \sum_{k\in\beta(j)} (q^c_{k,\phi} - q^g_{k,\phi}), \forall (i,j) \in \mathcal{E}, \forall \phi \in \Phi. \tag{10c}$$

Equation (10a) presents a linear relation between bus voltages and power injections and consumption $\mathbf{p^g}$, $\mathbf{p^c}$, $\mathbf{q^g}$, and $\mathbf{q^c}$, where $\mathbf{R} = [\mathbf{R}_{ij}]_{3N\times 3N}$ and $\mathbf{X} = [\mathbf{X}_{ij}]_{3N\times 3N}$ are the voltage sensitivity matrices. These matrices can be constructed following [30], [32]. Equations (10b) and (10c) indicate that the power flows through a cable (likewise the transformer) are calculated as the summation of net consumption of all downstream buses from the same phase, where $\beta(j)$ is defined as all descendants of bus j including itself [30]. The partial derivatives can now be calculated as:

$$\frac{\partial v_{i,\psi}}{\partial p_{j,\phi}} = \mathbf{R}_{i\psi,j\phi}, \frac{\partial v_{i,\psi}}{\partial q_{j,\phi}} = \mathbf{X}_{i\psi,j\phi}, \tag{11a}$$

$$\frac{\partial P_{mn,\psi}}{\partial p_{j,\phi}} = \frac{\partial Q_{mn,\psi}}{\partial q_{j,\phi}} = \begin{cases} -1 & \text{if } j \in \beta(n) \& \psi = \phi, \\ 0 & \text{otherwise,} \end{cases} \tag{11b}$$

$$\frac{\partial P_{trafo,\psi}}{\partial p_{j,\phi}} = \frac{\partial Q_{trafo,\psi}}{\partial q_{j,\phi}} = \begin{cases} -1 & \text{if } \psi = \phi, \\ 0 & \text{otherwise.} \end{cases} \tag{11c}$$

OFO algorithms have demonstrated robustness to such model approximation errors [21]–[23] due to its feedback-based implementation. Finally, the projection step (9c) ensures the feasibility of the active and reactive power setpoints.

Remark 3: Instead of relying on the grid model (10) to compute voltages and power flows, the algorithm incorporates measurements of voltages, as well as active and reactive power flows at cables of interest and the substation transformer as part of its feedback system. This creates a closed control loop, eliminating the necessity for precise distribution grid topologies and real-time data of non-controllable loads. This enhances robustness facing inaccurate problem data such as generation and load uncertainties, modeling errors, and intermittent and delayed communication.

Remark 4: The algorithm exhibits low computation and communication requirements, making it scalable to large grids. The gradient projection steps are performed locally and in parallel, including only basic arithmetic operators and small-scale convex quadratic programs. During each iteration, there are two communication rounds: initially, each bus sends updated Lagrangian multipliers to the DSO, followed by the DSO broadcasting all Lagrangian multipliers and power flow measurements for a few cables of interest and the transformer. Notably, the algorithm does not require user-specific generation and load data.

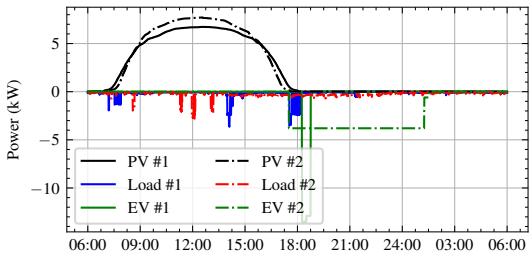

Fig. 3. Example PV generation, load, and EV profiles for two households #1 and #2. Positive values represent power injections, while negative values represent consumption.

Remark 5: The algorithm relies on input-output sensitivities to determine the optimal power setpoints, which reflects how voltages and power flows react to nodal power injections. This study leverages the linearized unbalanced power flow relations to compute the sensitivities offline, which works only for radial grids. By properly constructing sensitivity matrices through for example perturbations, as outlined in [33], the algorithm can also be applied effectively to meshed grids.

Remark 6: The gradient projection step (9c) involves solving a small-scale quadratic program locally, which outputs unique net nodal active and reactive power setpoints. However, this can be realized by the local PV, EV, and battery system in different ways. To obtain the final active and reactive power setpoints for individual DER, a new local small-scale optimization problem (12) is solved. The constraint ensures that the operational limits of individual DER are satisfied and the net nodal active and reactive power setpoints from (9c) are followed exactly. The objective function prioritizes PV energy harvest and EV demand fulfillment over discharging and charging of batteries respectively.

$$\begin{aligned} \max_{p^{pv},q^{pv},p^{ev},q^{ev},p^{ch},q^{ch}} \quad & p^{pv} + p^{ev} \\ \text{s. t. } & [p^{k+1}_{j,\phi}, q^{k+1}_{j,\phi}] \in \mathcal{X}^k_{j,\phi}. \end{aligned} \tag{12}$$

IV. Case Study

A. Case description

To evaluate the performance of the proposed multi-timescale coordinated control strategy, simulation studies are conducted on a 96-bus unbalanced low-voltage distribution grid with 6-second resolution generation and load data. The local optimization at the slower timescale is implemented with a 15-minute resolution. A 100% penetration scenario is studied for the three DER including PV, EV, and batteries. The distribution grid is adopted from Simbench [34] with a radial topology shown in Fig. 1. The substation transformer has a rated capability of 400 kVA. All households are assumed to evenly spread over different phases. PV capacities are uniformly generated from 3 to 10 kW. PV profiles are simulated using the *HelioClim-3* dataset [35] with a 1-minute resolution. The power ratings, energy demand, arrival, and departure data of EV are sampled with distributions from *ElaadNL Open Data* [36] for a weekday. The energy capacities of batteries

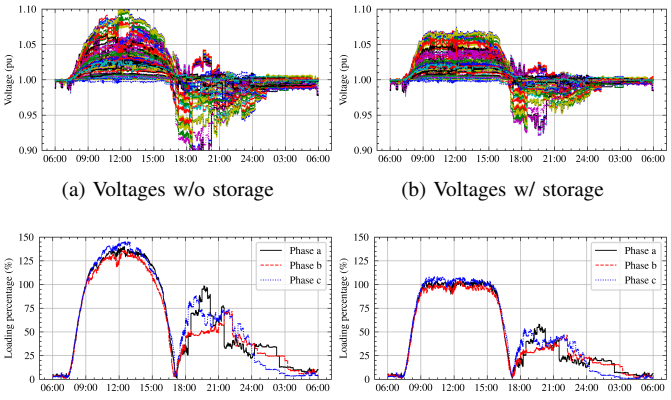

(a) Voltages w/o storage (b) Voltages w/ storage

(c) Loadings w/o storage (d) Loadings w/ storage

Fig. 4. Voltages and transformer loadings with/without battery storage.

(with a charging rate of 0.5C) are assumed to meet base load demand and 30% of the EV demand. The initial, minimum, and maximum SoC are taken as 0.2, 0.2, and 0.8, respectively. The charging and discharging efficiencies are both 98%. Finally, base load profiles are obtained by aggregating 1-second resolution profiles from the *ECO* dataset [37]. Fig. 3 visualizes two example PV, load, and EV profiles, showing their variability. High PV generation and EV charging demand can result in violated voltage limits and overloading of cables and transformers.

The voltage limits $\underline{v}$ and $\overline{v}$ are taken as 0.95 and 1.05 pu, respectively. The weighing factor ξ is chosen sufficiently small as 0.01. The step sizes for the PDGP algorithm are chosen with the trial and error strategy proposed in [9] as: $\alpha = 0.5$, $\alpha^{\lambda} = \alpha^{\mu} = 1 \times 10^{3}$, and $\alpha^{\rho} = \alpha^{\pi} = 100$. It should be noted that based on our experience, the algorithm works with a large range of those step sizes. An OFO iteration runs every 6 seconds, indicating that at each generation and load data point with a 6-second resolution, OFO runs once. Finally, the simulation runs from 6:00 am til 6:00 am the next day.

All simulations are performed on a standard PC with an Intel i7-9750H processor and a 16 GB RAM. Power flow calculations are implemented with a high-performance library PowerGridModel [38], [39]. Gurobi 10.0.1 [40] is used to solve optimization programs. The overall series implementation of the online feedback optimization framework takes around 28 minutes for a total of 14400 iterations, averaging less than 0.12 seconds for every iteration. This demonstrates its computational efficiency. In real-world implementation, the communication infrastructure and actuation speed of DER inverters can pose bottlenecks on the OFO update frequency.

B. Results

1) Local optimization: Fig. 4 shows bus voltages and transformer loading percentages with/without locally optimized battery storage profiles. In local optimization, batteries bridge PV generation and EV demand. Batteries store local surplus PV generation and use the stored energy to supply EV charging need. As expected, this significantly reduces voltage issues and transformer loadings. However, due to the limited battery capacities, voltage issues and transformer overloading are not entirely eliminated. This calls for real-time control to fully resolve voltage and congestion issues.

TABLE I
COMPARISON OF PV HARVEST AND EV CHARGING BETWEEN OUR PROPOSED APPROACH AND OPF. ALL UNITS IN KWH.

	PV harvest	PV curtailed	EV charge	EV unserved
Proposed	4562.4	42.1	1783.1	0.0
OPF	4543.4	61.1	1783.1	0.0

2) Real-time online feedback optimization: Given the reference setpoints computed in the local optimization stage, OFO controllers provide fast DER control to regulate voltages and asset loadings in real time. Fig. 5 shows voltages, asset loadings, and various DER profiles using OFO controllers. While temporally exceeded due to the corrective nature of OFO, voltage and asset loading limits are successfully enforced. Figs. 5d-5f show that batteries charge and discharge to absorb surplus PV generation and supply EV demand, respectively. When the energy capacities of batteries are reached, PV generation is noticeably curtailed to meet grid limits. The overshoots in battery charge profiles are caused by the saturation of EV demand. Once an EV is fully charged, it no longer draws power. Nevertheless, it takes some time for the net nodal power injection setpoints to increase (drawing less power), which results in temporary charging of the batteries.

3) Benchmark with optimal power flow: To assess the solution quality of the proposed strategy, a multi-period centralized OPF approach is used for benchmark purposes. We introduce several assumptions to attain the tractability of the centralized OPF problem. First, we assume 100% charging and discharging efficiencies, eliminating the need for binary variables to prevent simultaneous charge and discharge. Second, we use 15-minute resolution data with averaged generation and demand values to manage the problem size. Note that these two assumptions are also applied to obtain results of OFO for a fair comparison. Finally, we leverage the linearized power flow relations and assume accurate knowledge of grid topology and generation and load profiles. The OPF model is solved offline once to get results for all time steps during the simulation horizon, representing a perfect-information case for a model-based method. Since both approaches effectively address voltage and congestion issues, we evaluate their performance based on key indicators including the total PV energy yield and the satisfaction of EV demand. Table I shows that while both approaches result in negligible unserved EV demand, our proposed approach leads to slightly more PV energy harvest. Comparing Figs. 5a, 5c, and 6, we find that our proposed approach utilizes existing grid capacities more efficiently than OPF. By leveraging measurements as feedback, OFO controllers can maximize the utilization of grid capacities. In contrast, OPF, relying on approximate grid models, results in voltage and asset loading headrooms. To summarize, our proposed multi-timescale approach, while not requiring precise distribution grid topologies or intrusive

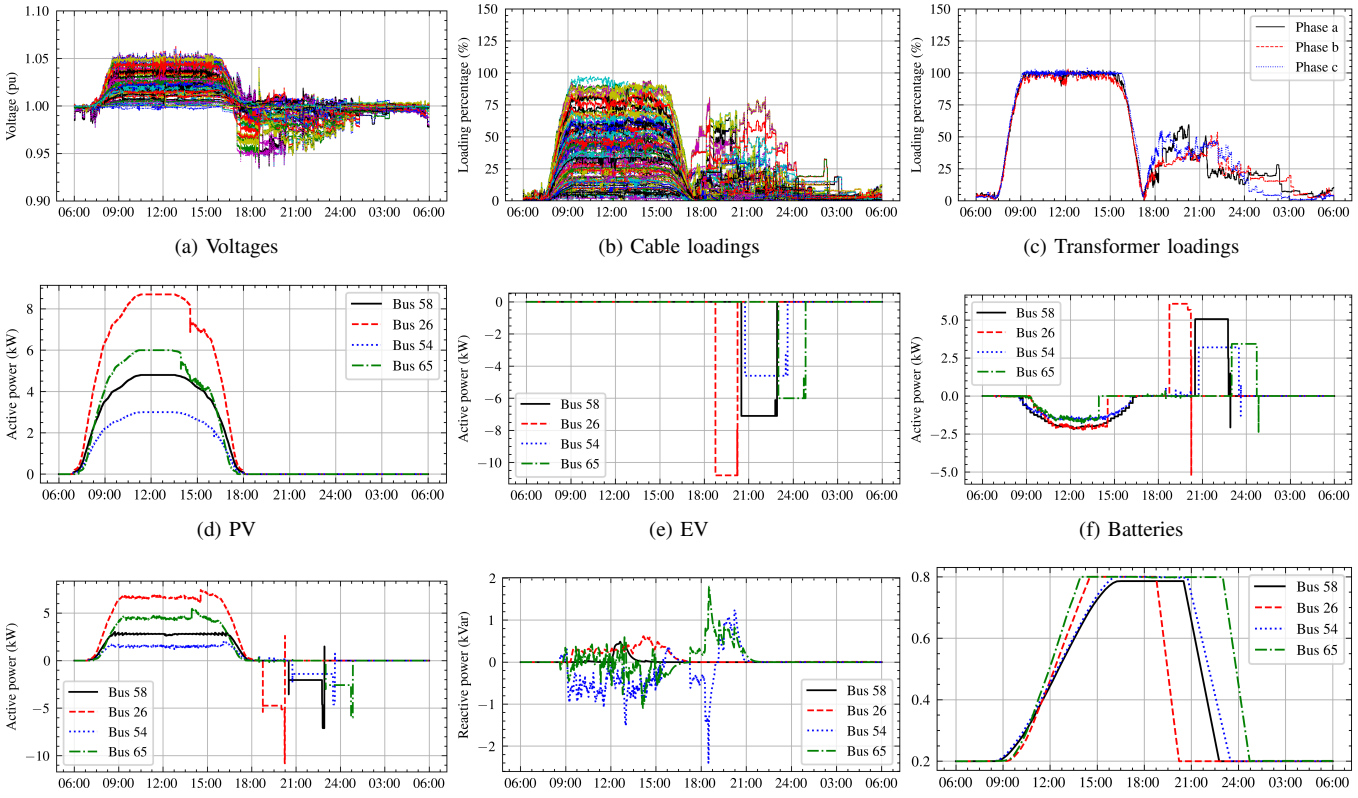

(a) Voltages (b) Cable loadings (c) Transformer loadings

(d) PV (e) EV (f) Batteries

(g) Net active power injections (h) Net reactive power injections (i) Battery SoC

Fig. 5. Grid states and DER profiles with real-time OFO controllers. Positive values represent power injections, while negative values represent consumption.

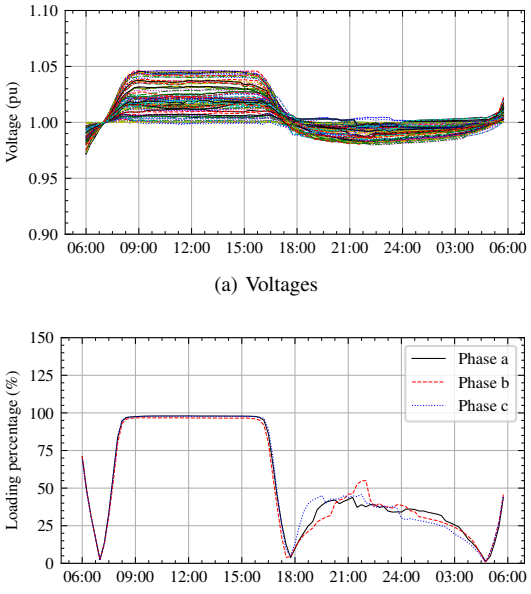

(a) Voltages

(b) Transformer loadings

Fig. 6. Grid states using centralized optimal power flow.

load metering of end-users, and having light computation and communication requirements, demonstrates efficient utilization of DER also with short-term planning capabilities.

V. Conclusion

In this study, we proposed a multi-timescale coordinated strategy integrating local optimization and OFO for distribution grid management. Using reference setpoints computed with local optimization, OFO controllers make an efficient use of DER with short-term planning capabilities, which is demonstrated with improved PV energy harvest and fully satisfied EV demand. The overall approach does not require precise grid topologies or intrusive load metering, has minimum computation and communication requirements, and guarantees compliance with grid limits. These characteristics make it highly applicable to manage distribution grids.

While this paper advocated the use of local optimization due to its light communication and computation requirements and reduced privacy concerns, optimal power flow methods remain a viable option for potentially better coordination of various DER in the slower timescale with *ideal* grid conditions: perfect knowledge of topology, accurate generation and load forecast, and advanced communication infrastructure. The slower timescale optimization can also be solved on a rolling basis leveraging the most recent forecast. Furthermore, these DER can be planned for economic benefits, which might exacerbate congestion issues in local distribution grids. OFO controllers can consequently be used to ensure grid safety in real time while tracking economically favorable DER setpoints, integrating markets and control.

REFERENCES

[1] S. Bolognani, R. Carli, G. Cavraro, and S. Zampieri, "Distributed reactive power feedback control for voltage regulation and loss minimization," *IEEE Trans. Automat. Contr.*, vol. 60, no. 4, pp. 966–981, 2015.

[2] H. Zhu and H. J. Liu, "Fast local voltage control under limited reactive power : Optimality and stability analysis," *IEEE Trans. Power Syst.*, vol. 31, no. 5, 2016.

[3] Y. Tang, K. Dvijotham, and S. Low, "Real-time optimal power flow," *IEEE Trans. Smart Grid*, vol. 8, no. 6, 2017.

[4] E. Dall'Anese and A. Simonetto, "Optimal power flow pursuit," *IEEE Trans. Smart Grid*, vol. 9, no. 2, 2018.

[5] A. Bernstein and E. Dall'Anese, "Real-time feedback-based optimization of distribution grids: A unified approach," *IEEE Trans. Control Netw. Syst.*, vol. 6, no. 3, 2019.

[6] M. Colombino, J. W. Simpson-Porco, and A. Bernstein, "Towards robustness guarantees for feedback-based optimization," in *Proc. IEEE Conf. Decis. Control*. IEEE, 2019, pp. 6207–6214.

[7] S. Bolognani, R. Carli, G. Cavraro, and S. Zampieri, "On the need for communication for voltage regulation of power distribution grids," *IEEE Trans. Control Netw. Syst.*, vol. 6, no. 3, pp. 1111–1123, 2019.

[8] M. Picallo, S. Bolognani, and F. Dörfler, "Closing the loop: Dynamic state estimation and feedback optimization of power grids," *Electr. Power Syst. Res.*, vol. 189, 2020.

[9] G. Qu and N. Li, "Optimal distributed feedback voltage control under limited reactive power," *IEEE Trans. Power Syst.*, vol. 35, no. 1, 2020.

[10] A. Hauswirth, S. Bolognani, G. Hug, and F. Dörfler, "Optimization algorithms as robust feedback controllers," *arXiv*, 2021.

[11] Z. Tang, D. J. Hill, and T. Liu, "Distributed coordinated reactive power control for voltage regulation in distribution networks," *IEEE Trans. Smart Grid*, vol. 12, no. 1, 2021.

[12] S. Zhan, J. Morren, W. van den Akker, A. van der Molen, N. G. Paterakis, and J. G. Slootweg, "Fairness-incorporated online feedback optimization for real-time distribution grid management," *IEEE Trans. Smart Grid*, vol. 15, no. 2, pp. 1792–1806, 2024.

[13] S. Zhan, I. Dukovska, W. van den Akker, A. van der Molen, J. Morren, N. G. Paterakis, and J. Slootweg, "Review of recent developments in technical control approaches for voltage and congestion management in distribution networks," in *IEEE PowerTech*, 2023.

[14] V. Bassi, L. F. Ochoa, T. Alpcan, and C. Leckie, "Electrical model-free voltage calculations using neural networks and smart meter data," *IEEE Trans. Smart Grid*, no. December, 2022.

[15] M. Picallo, L. Ortmann, S. Bolognani, and F. Dörfler, "Adaptive real-time grid operation via online feedback optimization with sensitivity estimation," *Electr. Power Syst. Res.*, vol. 212, 2022.

[16] R. Cheng, Z. Wang, and Y. Guo, "An online feedback-based linearized power flow model for unbalanced distribution networks," *IEEE Trans. Power Syst.*, vol. 37, no. 5, pp. 3552–3565, 2022.

[17] T. Xu, W. Wu, Y. Hong, J. Yu, and F. Zhang, "Data-driven inverter-based volt/var control for partially observable distribution networks," *CSEE J. Power Energy Syst.*, vol. 9, no. 2, pp. 548–560, 2023.

[18] Y. Chen, A. Bernstein, A. Devraj, and S. Meyn, "Model-free primal-dual methods for network optimization with application to real-time optimal power flow," in *Proc. Am. Control Conf.*, no. 5, 2020, pp. 3140–3147.

[19] Z. He, S. Bolognani, J. He, F. Dörfler, and X. Guan, "Model-free nonlinear feedback optimization," *IEEE Trans. Automat. Contr.*, vol. PP, pp. 1–16, 2022.

[20] C. Hu, X. Zhang, and Q. Wu, "Gradient-free accelerated event-triggered scheme for constrained network optimization in smart grids," *IEEE Trans. Smart Grid*, 2023.

[21] S. Magnússon, G. Qu, and N. Li, "Distributed optimal voltage control with asynchronous and delayed communication," *IEEE Trans. Smart Grid*, vol. 11, no. 4, 2020.

[22] N. Patari, A. K. Srivastava, and N. Li, "Distributed optimal voltage control considering latency and asynchronous communication for three phase unbalanced distribution systems," *IEEE Trans. Power Syst.*, 2022.

[23] L. Ortmann, A. Hauswirth, I. Cadu, F. Dörfler, and S. Bolognani, "Experimental validation of feedback optimization in power distribution grids," *Electr. Power Syst. Res.*, vol. 189, 2020.

[24] L. Ortmann, A. Prostejovsky, K. Heussen, and S. Bolognani, "Fully distributed peer-to-peer optimal voltage control with minimal model requirements," *Electr. Power Syst. Res.*, vol. 189, p. 106717, 2020.

[25] L. Ortmann, C. Rubin, A. Scozzafava, J. Lehmann, S. Bolognani, and F. Dörfler, "Deployment of an online feedback optimization controller for reactive power flow optimization in a distribution grid," in *IEEE PES Innov. Smart Grid Technol. Conf. Eur.*, 2023.

[26] N. Kelepouris, A. Nousdilis, A. Bouhouras, and G. Christoforidis, "Optimal scheduling of prosumer's battery storage and flexible loads for distribution network support," *IET Gener. Transm. Distrib.*, 2023.

[27] M. E. Gerards, H. A. Toersche, G. Hoogsteen, T. van der Klauw, J. L. Hurink, and G. J. Smit, "Demand side management using profile steering," in *IEEE Eindhoven PowerTech*. IEEE, 2015.

[28] C. Zhang and Y. Xu, "Hierarchically-coordinated voltage/var control of distribution networks using pv inverters," *IEEE Trans. Smart Grid*, vol. 11, no. 4, 2020.

[29] C. Zhang, Y. Xu, Z. Dong, and J. Ravishankar, "Three-stage robust inverter-based voltage/var control for distribution networks with high-level PV," *IEEE Trans. Smart Grid*, vol. 10, no. 1, 2019.

[30] M. Farivar, L. Chen, and S. Low, "Equilibrium and dynamics of local voltage control in distribution systems," 2013.

[31] L. Gan and S. H. Low, "Convex relaxations and linear approximation for optimal power flow in multiphase radial networks," in *Proc. - 2014 Power Syst. Comput. Conf. PSCC*, 2014.

[32] R. Cheng, Z. Wang, Y. Guo, and Q. Zhang, "Online voltage control for unbalanced distribution networks using projected newton method," *IEEE Trans. Power Syst.*, 2022.

[33] A. Fu, M. Cvetkovi´c, and P. Palensky, "Distributed cooperation for voltage regulation in future distribution networks," *IEEE Trans. Smart Grid*, 2022.

[34] S. Meinecke, D. Sarajlić, S. R. Drauz, A. Klettke, L. P. Lauven, C. Rehtanz, A. Moser, and M. Braun, "Simbench-a benchmark dataset of electric power systems to compare innovative solutions based on power flow analysis," *Energies*, vol. 13, no. 12, 2020.

[35] Helioclim-3 solar radiation. [Online]. Available: https://www.soda-pro.com/web-services/radiation/helioclim-3-archives-for-free

[36] Elaadnl. [Online]. Available: https://platform.elaad.io/analyses.html

[37] C. Beckel, W. Kleiminger, R. Cicchetti, T. Staake, and S. Santini, "The ECO data set and the performance of non-intrusive load monitoring algorithms," in *BuildSys '14*, 2014.

[38] Y. Xiang, P. Salemink, B. Stoeller, N. Bharambe, and W. van Westering, "Power Grid Model: A high-performance distribution grid calculation library," in *27 th Int. Conf. Electr. Distrib. (CIRED)*, no. June, 2023.

[39] Y. Xiang, P. Salemink, N. Bharambe, M. Govers, J. van den Bogaard, B. Stoeller, L. Jagutis, C. Wang, and Contributors from the LF Energy project Power Grid Model, "PowerGridModel/power-grid-model." [Online]. Available: https://github.com/PowerGridModel/power-grid-model

[40] Gurobi Optimization, LLC, "Gurobi optimizer reference manual," 2023. [Online]. Available: https://www.gurobi.com